Recent Progress on the Determination of the Symmetry Energy

CHEN Liewen[1, 2]

(1. Department of Physics and Astronomy, Shanghai Jiao Tong University, Shanghai 200240, China;

2. Center of Theoretical Nuclear Physics, National Laboratory of Heavy-Ion Accelerator, Lanzhou 730000, China)

Abstract: We summarize the current available constraints on the density dependence of the symmetry energy obtained from terrestrial laboratory measurements and astrophysical observations. While the magnitude $E_{\text{sym}}(\rho_0)$ and density slope L of the symmetry energy at saturation density ρ_0 can vary largely depending on the data or analysis methods, all the available constraints are in agreement with $E_{\text{sym}}(\rho_0) = (32.5 \pm 2.5)$ MeV and $L = (55 \pm 25)$ MeV. The determination of the high density behaviors of the symmetry energy remains a big challenge.

Key words: symmetry energy; equation of state for asymmetric nuclear matter; nuclear reaction; nuclear structure; neutron star

1 Introduction

In the current research frontiers of nuclear physics and astrophysics, there is of great interest to determine the density dependence of the nuclear symmetry energy $E_{\text{sym}}(\rho)$ that essentially characterizes the isospin dependent part of the equation of state (EOS) of asymmetric nuclear matter. The exact knowledge on the symmetry energy is critically important for understanding not only a number of questions in nuclear physics, such as the structure of radioactive nuclei, the reaction dynamics induced by rare isotopes, the liquid-gas phase transition in asymmetric nuclear matter, and the isospin dependence of QCD phase diagram, but also many interesting issues such as the properties of neutron stars and the explosion mechanism of supernova in astrophysics[1–8]. The symmetry energy may also involve some interesting issues regarding possible new

physics beyond the standard model[9–11]. During the last decade, although significant progress has been made both experimentally and theoretically on constraining the density dependence of the symmetry energy[2–8], mainly based on the data analysis from terrestrial laboratory measurements and astrophysical observations, large uncertainties on $E_{\text{sym}}(\rho)$ still exist, especially its high density behavior remains largely uncertain[12–15]. To more accurately determine the density dependence of the nuclear symmetry energy thus provides a strong motivation for studying isospin nuclear physics in radioactive nuclei at the new/planning rare isotope beam facilities around the world, such as CSR/IMP and BRIF-II/CIAE in China, RIBF/RIKEN in Japan, SPIRAL2/GANIL in France, FAIR/GSI in Germany, FRIB/NSCL and T-REX/TAMU in USA, SPES/LNL in Italy, and RAON in Korea.

Biography: CHEN Liewen(1971–), male, Hunan, China, Professor, working on the field of theoretical nuclear physics, E-mail: lwchen@sjtu.edu.cn.

Based on a previous report[16], in the present paper, we revise and update the current status on constraining the density dependence of the symmetry energy from the analysis of terrestrial laboratory measurements and astrophysical observations, mainly including nuclear reactions, nuclear structures, and the properties of neutron stars. In particular, we will focus on heavy ion collisions, nuclear optical model potential, nuclear mass, nuclear neutron skin thickness and pygmy dipole resonance, the mass and radius of neutron stars, and the crust oscillations and r-mode instability of neutron stars.

2　The symmetry energy

The EOS of isospin asymmetric nuclear matter, defined by its binding energy per nucleon, can be expanded to 2nd-order in isospin asymmetry δ as

$$E(\rho, \delta) = E_0(\rho) + E_{\mathrm{sym}}(\rho)\delta^2 + O(\delta^4) , \qquad (1)$$

where $\rho = \rho_{\mathrm{n}} + \rho_{\mathrm{p}}$ is the baryon density with ρ_{n} and ρ_{p} denoting the neutron and proton densities, respectively; $\delta = (\rho_{\mathrm{n}} - \rho_{\mathrm{p}})/(\rho_{\mathrm{p}} + \rho_{\mathrm{n}})$ is the isospin asymmetry; $E_0(\rho) = E(\rho, \delta = 0)$ is the binding energy per nucleon in symmetric nuclear matter, and the symmetry energy is expressed as

$$E_{\mathrm{sym}}(\rho) = \frac{1}{2!} \frac{\partial^2 E(\rho, \delta)}{\partial \delta^2}\Big|_{\delta=0} . \qquad (2)$$

Neglecting the contribution from higher-order terms in Eq. (1) leads to the well-known empirical parabolic law for the EOS of asymmetric nuclear matter, which has been verified by all many-body theories to date, at least for densities up to moderate values[5, 17]. As a good approximation, therefore, the density-dependent symmetry energy $E_{\mathrm{sym}}(\rho)$ can be extracted from the parabolic approximation as

$$E_{\mathrm{sym}}(\rho) \approx E(\rho, \delta = 1) - E(\rho, \delta = 0) . \qquad (3)$$

Around the saturation density ρ_0, the nuclear symmetry energy $E_{\mathrm{sym}}(\rho)$ can be expanded, e.g., up to 2nd-order in density, as

$$E_{\mathrm{sym}}(\rho) = E_{\mathrm{sym}}(\rho_0) + L\chi + \frac{K_{\mathrm{sym}}}{2!}\chi^2 + O(\chi^3) , \quad (4)$$

where $\chi = (\rho - \rho_0)/3\rho_0$ is a dimensionless variable characterizing the deviations of the density from ρ_0,

and L and K_{sym} are the slope parameter and curvature parameter, respectively, i.e.,

$$L = 3\rho_0 \frac{\mathrm{d}E_{\mathrm{sym}}(\rho)}{\partial \rho}\Big|_{\rho=\rho_0} , \qquad (5)$$

$$K_{\mathrm{sym}} = 9\rho_0^2 \frac{\mathrm{d}^2 E_{\mathrm{sym}}(\rho)}{\partial \rho^2}\Big|_{\rho=\rho_0} . \qquad (6)$$

3　The symmetry energy around the saturation density

During the last decade, a number of experimental probes have been proposed to constrain the density dependence of the symmetry energy. Most of them are for the symmetry energy around the saturation density while a few of probes are for the suprasaturation density behaviors. In this section, we summarize the current status on constraining the symmetry energy around the saturation density, mainly, the parameters $E_{\mathrm{sym}}(\rho_0)$ and L, from nuclear reactions, nuclear structures, and the properties of neutron stars.

3.1　Nuclear reactions

Nuclear reactions, mainly including heavy ion collisions and nucleon-nucleus scattering, provide an important tool to explore the density dependence of the symmetry energy.

3.1.1　Heavy ion collisions

One important progress on constraining the density dependence of the symmetry energy is from the isospin dependent Boltzmann-Uehling-Uhlenbeck (IBUU04) transport model analysis[18] on the isospin diffusion data from NSCL-MSU[19]. It is found that the degree of isospin diffusion in heavy-ion collisions is affected by both the stiffness of the nuclear symmetry energy and the momentum dependence of the nucleon potential. Using a momentum dependence derived from the Gogny effective interaction and the corresponding isospin dependent in-medium nucleon-nucleon scattering cross sections, the experimental data from NSCL-MSU on isospin diffusion in collisions at $E/A = 50$ MeV involving ^{112}Sn and ^{124}Sn nuclei leads to a constraint of $L = (86 \pm 25)$ MeV with $E_{\mathrm{sym}}(\rho_0) = 30.5$ MeV[18, 20], which is shown as a solid square with error bar labeled "Iso. Diff. (IBUU04, 2005)" in Fig. 1. It

should be mentioned that the constraint in the original publication[18, 20] is $L = (88 \pm 25)$ MeV and $E_{\mathrm{sym}}(\rho_0) = 31.6$ MeV, due to the application of the parabolic approximation Eq. (3) for the symmetry energy. This constraint is significantly softer than the prediction by transport model simulation with momentum-independent interaction[19] and in agreement with microscopic theoretical calculations.
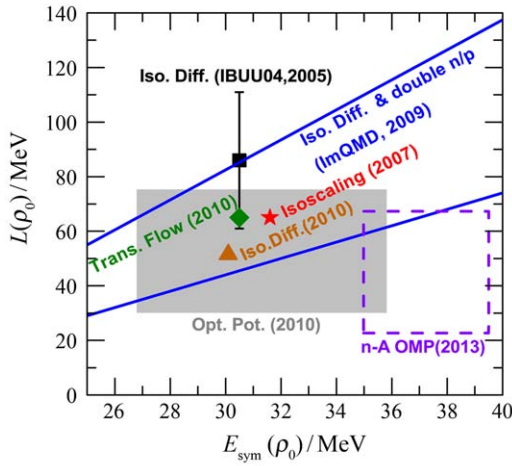

Fig. 1　(color online) Constraints on $E_{\mathrm{sym}}(\rho_0)$ and L from heavy ion collisions and nuclear optical model potentials. See text for details.

Another progress is from the analysis of the isoscaling of the fragment yields in heavy ion collisions, which has been shown to be a good probe of the symmetry energy[21]. By analyzing the isoscaling of the fragment yields in Ar+Fe/Ca+Ni, Fe+Fe/Ni+Ni, Ar+Ni/Ca+Ni, and Fe+Ni/Ni+Ni reactions at Fermi energy region, within the antisymmetrized molecular dynamic (AMD) model, a extraction of $E_{\mathrm{sym}}(\rho_0) = 31.6$ MeV and $L = 65$ MeV has been obtained in Ref. [22], which is denoted by a solid star with a label "Isoscaling (2007)" in Fig. 1.

In heavy ion collisions, the double ratios of neutron and proton energy spectra also provide a good probe of the symmetry energy. An improved quantum molecular dynamics (ImQMD) transport model analysis[23] of the isospin diffusion data from two different observables and the ratios of neutron and proton spectra in collisions at $E/A = 50$ MeV involving ^{112}Sn and ^{124}Sn nuclei has led to a constraint on $E_{\mathrm{sym}}(\rho_0)$ and L at 95% confidence level, corresponding to 2 standard deviations from the mini-

mum χ^2. This constraint is denoted by the region between two solid lines with a label "Iso. Diff. & double n/p (ImQMD, 2009)" in Fig. 1. A more recent ImQMD model analysis[24] of the isospin diffusion data from heavy ion collisions at lower incident energy ($E/A = 35$ MeV) involving ^{112}Sn and ^{124}Sn nuclei has led to a constraint of $E_{\mathrm{sym}}(\rho_0) = 30.1$ MeV and $L = 51.5$ MeV, which is shown by solid up-triangle with a label "Iso. Diff. (2010)" in Fig. 1.

The isospin effects of fragment transverse flows in heavy ion collisions provide another useful probe for extracting information on the symmetry energy. In a recent work[25], the transverse flow of intermediate mass fragments (IMFs) has been investigated for the 35 MeV/u ^{70}Zn + ^{70}Zn, ^{64}Zn + ^{64}Zn, and ^{64}Ni + ^{64}Ni systems. The analysis based on the AMD model with the GEMINI code treatment for statistically de-excitation of the hot fragments leads to a constraint $E_{\mathrm{sym}}(\rho_0) = 30.5$ MeV and $L = 65$ MeV, which is shown by solid diamond with a label "Trans. Flow (2010)" in Fig. 1.

3.1.2　Nucleon optical potential

Experimentally, there have accumulated a lot of data for elastic scattering of proton (and neutron) from different targets at different beam energies and (p,n) charge-exchange reactions between isobaric analog states. These data provide the possibility to extract information on the isospin dependence of the nucleon optical potential, especially the energy dependence of the nuclear symmetry potential. Based on the Hugenholtz-Van Hove theorem, it has been shown recently[26–29] that both $E_{\mathrm{sym}}(\rho_0)$ and L can be completely and analytically determined by the nucleon optical potentials. Averaging all nuclear symmetry potentials constrained by world data available in the literature since 1969 from nucleon-nucleus scatterings, (p,n) charge-exchange reactions, and single-particle energy levels of bound states, the constraint $E_{\mathrm{sym}}(\rho_0) = (31.3 \pm 4.5)$ MeV and $L = (52.7 \pm 22.5)$ MeV are simultaneously obtained[26], and this constraint is indicated by the gray band with a label "Opt. Pot. (2010)" in Fig. 1.

More recently, using the available experimental data from neutron-nucleus scatterings[30−31], a new

set of the global isospin dependent neutron-nucleus optical model potential parameters, which include the nuclear symmetry potential up to the second order in isospin asymmetry for the first time, has been obtained. Based on this new global isospin dependent neutron-nucleus optical model potential parameters, the constraint $E_{\mathrm{sym}}(\rho_0) = (37.24 \pm 2.26)$ MeV and $L = (44.98 \pm 22.31)$ MeV are simultaneously obtained[31], and this constraint is shown by a square box with dashed-line sides labeled "n-A OMP (2013)" in Fig. 1.

3.2 Nuclear structures

In recent years, more and more constraints on the symmetry energy around saturation density have been obtained from the analyses of nuclear structure properties, such as the nuclear mass (ground state binding energy), the neutron skin thickness, the nuclear isobaric analog state energies, and pygmy dipole resonances. We summarize these constraints in the following.

3.2.1 Nuclear mass

The data of nuclear mass are probably the most accurate, richest, and least ambiguous in the nuclear data library. The Thomas-Fermi model analysis[32] of 1654 ground state mass of nuclei with $N, Z \geqslant 8$ has given rise to $E_{\mathrm{sym}}(\rho_0) = 32.65$ MeV and $L = 49.9$ MeV, which is shown by solid star with a label "TF+Nucl. Mass (1996)" in Fig. 2.
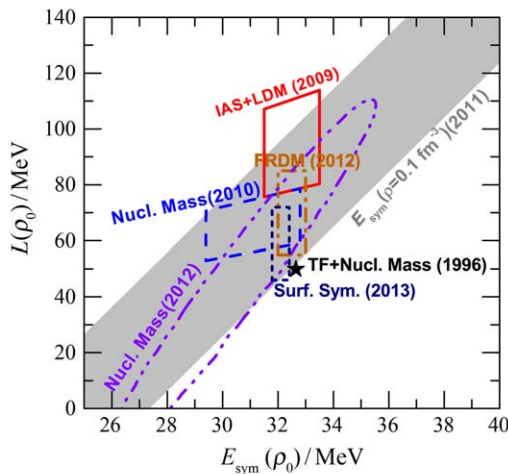

Fig. 2 (color online) Constraints on $E_{\mathrm{sym}}(\rho_0)$ and L from nuclear mass and isobaric analog state. See text for details.

The symmetry energy coefficients $a_{\mathrm{sym}}(A)$ of finite nuclei with mass numbers $A = 20 \sim 250$ were determined from more than 2000 precisely measured nuclear masses[33]. With the semiempirical connection between $a_{\mathrm{sym}}(A)$ and the symmetry energy at reference densities ρ_A, i.e., $E_{\mathrm{sym}}(\rho_A) \approx a_{\mathrm{sym}}(A)$, and assuming a symmetry energy with density dependence of $E_{\mathrm{sym}}(\rho) = E_{\mathrm{sym}}(\rho_0)(\rho/\rho_0)^{\gamma}$, Liu et al.[33] obtained a constraint at 95% confidence level shown as a parallelogram with dashed-line sides in Fig. 2, labeled "Nucl. Mass (2010)".

Within the Skyrme-Hartree-Fock (SHF) approach, it has been shown recently that a value of $E_{\mathrm{sym}}(\rho_A)$ at a subsaturation reference density ρ_A leads to a positive linear correlation between $E_{\mathrm{sym}}(\rho_0)$ and L[34]. Using recently extracted $E_{\mathrm{sym}}(\rho_A = 0.1~\mathrm{fm}^{-3}) \approx a_{\mathrm{sym}}(A = 208) = 20.22 \sim 24.74$ MeV at 95% confidence level from more than 2000 measured nuclear masses, Chen[34] obtained a constraint denoted by the gray band with a label "$E_{\mathrm{sym}}(\rho_A = 0.1~\mathrm{fm}^{-3})(2011)$" in Fig. 2.

The finite-range droplet model (FRDM) has been shown to be very successful to describe the nuclear ground state mass. The parameters in the macroscopic droplet part of the FRDM are related to the properties of the equation of state. Using the new, more accurate FRDM-2011a version, Moller et al.[35] analyzed the nuclear mass of the 2003 Atomic Mass Evaluation (AME2003), and obtained the constraint $E_{\mathrm{sym}}(\rho_0) = (32.5 \pm 0.5)$ MeV and $L = (70 \pm 15)$ MeV shown as a square box bounded by dash-dotted lines in Fig. 2, labeled "FRDM (2012)".

In a recent work[36], Lattimer and Lim used the confidence ellipse method for nuclear mass fitting. Based on a SHF energy-density functional for nuclear masses, they obtained a 95% confidence ellipse for the $E_{\mathrm{sym}}(\rho_0) - L$ constraints shown by the dash-dot-dotted lines in Fig. 2, labeled "Nucl. Mass (2012)".

In addition, using some precise empirical values of the nuclear volume and surface symmetry energy coefficients and the nuclear saturation density, i.e., $E_{\mathrm{sym}}(\rho_0) = (32.10 \pm 0.5)$ MeV and $C_{\mathrm{s}} = (58.91 \pm 1.08)$ MeV[37] as well as $\rho_0 = (0.155 \pm 0.008)~\mathrm{fm}^{-3}$, Agrawal et al.[38] extracted a value of $L = (59 \pm 13)$ MeV shown

as a square box bounded by short-dashed lines in Fig. 2, labeled "Surf. Sym. (2013)".

3.2.2　Nuclear isobaric analog state energies

The nuclear isobaric analog state (IAS) energies are believed to provide a particularly clean and useful probe of the symmetry energy since the ambiguities in the determination of the symmetry energy of finite nuclei from binding energies caused by the Coulomb term can be removed[39]. By fitting the available data on the IAS and using the droplet surface symmetry energy, Danielewicz and Lee[40] obtained the constraint shown as a parallelogram bounded by solid lines in Fig. 2, labeled "IAS+LDM (2009)".

3.2.3　Neutron skin thickness

Theoretically, it has been established[20, 41] that the neutron skin thickness of heavy nuclei, given by the difference of their neutron and proton root-mean-squared radii, provides a good probe of $E_{sym}(\rho)$. Based on the droplet model, Centelles et al.[42] analyzed the neutron skin sizes measured in 26 antiprotonic atoms along the mass table, and they obtained the constraint $E_{sym}(\rho_0) = 28 \sim 35$ MeV and $L = 30 \sim 80$ MeV shown as a square box bounded by dashed lines in Fig. 3, labeled "DM+N-Skin (2009)".
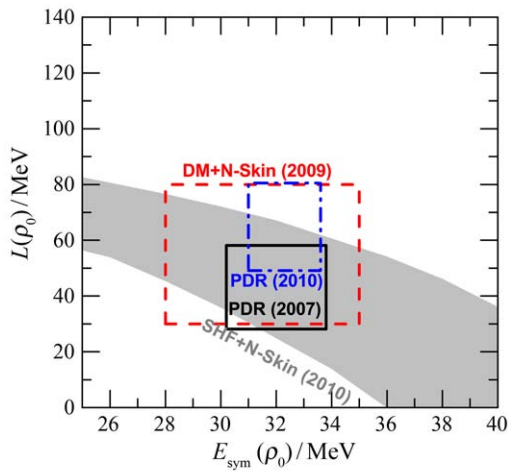

Fig. 3　(color online) Constraints on $E_{sym}(\rho_0)$ and L from nuclear neutron skin thickness and pygmy dipole resonance. See text for details.

Using a new correlation analysis method within the microscopic SHF approach, Chen et al.[43] analyzed the neutron skin thickness of Sn isotopes, and

they obtained a set of constraints corresponding to 95% confidence levels, shown as a gray band in Fig. 3, labeled "SHF+N-Skin (2010)".

3.2.4　Pygmy dipole resonance

The experimentally observed pygmy dipole (E1) strength might play an equivalent role as the neutron rms radius in constraining the symmetry energy[44]. Excess neutrons forming the skin give rise to pygmy dipole transitions at excitation energies below the giant dipole resonance, and such transitions could represent a collective vibration of excess neutrons against an isospin symmetric core. Comparing the measured pygmy dipole strength in ^{130,132}Sn to that obtained within a relativistic mean-field approach, Klimkiewicz et al.[45] obtained the constraint $E_{sym}(\rho_0) = 30.2 \sim 33.8$ MeV and $L = 28.1 \sim 58.1$ MeV shown as a square box bounded by solid lines in Fig. 3, labeled "PDR (2007)". Another analysis by Carbone et al.[46] on the measured pygmy dipole strength in ^{68}Ni and ^{132}Sn within the relativistic and non-relativistic mean-field approaches leads to the constraint $E_{sym}(\rho_0) = 31.0 \sim 33.6$ MeV and $L = 49.1 \sim 80.5$ MeV shown as a square box bounded by dash-dotted lines in Fig. 3, labeled "PDR (2010)".

3.3　The properties of neutron stars

In recent years, more and more constraints on the symmetry energy have been available from the analyses of astrophysical observations on the properties of neutron stars, such as the mass and radius of neutron stars, the gravitational binding energy, crust oscillations and r-mode instability of neutron stars. We summarize these constraints in the following.

3.3.1　Mass and radius of neutron stars

Astrophysical observations of neutron star masses and radii provide important probe for the EOS of neutron-rich matter. In particular, neutron star radii have been found to strongly correlate with neutron matter pressures around the saturation density[47].

Based on a heterogeneous data set of six neutron stars and using a Markov chain Monte Carlo algorithm within a Bayesian framework, together with the assumption that the interaction part of the symmetry energy has the density dependence of $(\rho/\rho_0)^\gamma$,

Steiner, Lattimer, and Brown[48] obtained the 1σ uncertainty constraint $E_{\mathrm{sym}}(\rho_0) = 28.1 \sim 34.4$ MeV and $L = 40.7 \sim 55.4$ MeV if $r_{\mathrm{ph}} \gg R$ is assumeed (r_{ph} is the photospheric radius at the time the flux is evaluated, and R is the stellar radius), which is shown as a square box bounded by solid lines in Fig. 4, labeled "NS-MR-SLB-a (2010)". If $r_{\mathrm{ph}} = R$ is assumed, the constraint then changes to $E_{\mathrm{sym}}(\rho_0) = 28.7 \sim 37.1$ MeV and $L = 41.0 \sim 71.4$ MeV shown as a square box bounded by dashed lines in Fig. 4, labeled "NS-MR-SLB-b (2010)".
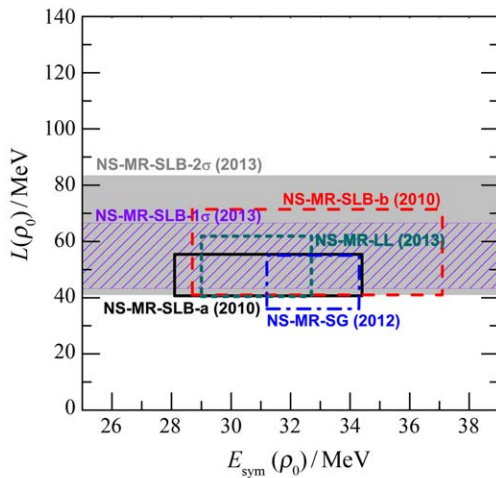

Fig. 4　(color online) Constraints on $E_{\mathrm{sym}}(\rho_0)$ and L from mass and radius of neutron stars. See text for details.

In a recent work[49], Steiner and Gandolfi demonstrated that currently available neutron star mass and radius measurements provide a significant constraint on the EOS of pure neutron matter. Using a phenomenological parametrization for EOS of neutron matter near and above the saturation density with partial parameters determined by the quantum Monte Carlo calculations, they obtained a constraint of $E_{\mathrm{sym}}(\rho_0) = 31.2 \sim 34.3$ MeV and $L = 36 \sim 55$ MeV at 95% confidence level based on Bayesian analysis[6, 49], and this constraint is shown as a square box bounded by dash-dotted lines in Fig. 4, labeled "NS-MR-SG (2012)". More recently, Lattimer and Lim[36] performed a similar Bayesian analysis of the available neutron star mass and radius measurements, they obtained a constraint of $E_{\mathrm{sym}}(\rho_0) = 29.0 \sim 32.7$ MeV and $L = 40.5 \sim 61.9$

MeV shown as a square box bounded by short-dashed lines in Fig. 4, labeled "NS-MR-LL (2013)".

In addition, based on recent observations of both transiently accreting and bursting sources and using the Bayesian analysis, Steiner, Lattimer, and Brown[50] more recently obtained the constraint $L = 43.3 \sim 65.5$ MeV to 68% confidence and $L = 41.1 \sim 83.4$ MeV to 95% confidence for L alone as their analysis cannot place effective constraints on the $E_{\mathrm{sym}}(\rho_0)$, and they are shown as gray band (labeled "NS-MR-SLB-2σ (2013)") and slanted-line band (labeled "NS-MR-SLB-1σ (2013)"), respectively, in Fig. 4.

3.3.2 The gravitational binding energy, crust oscillations and r-mode instability of neutron stars

Besides neutron star mass and radius, other properties of neutron stars such as the gravitational binding energy, crust oscillations and r-mode instability, may also put constraints on the symmetry energy[51].

Indeed, Newton and Li[52] have demonstrated that the gravitational binding energy of a neutron star for a given mass is correlated with the slope of the nuclear symmetry energy around the nuclear saturation density. By analyzing the double pulsar binary system PSR J0737-3039B, and assuming that it comes from an electron capture supernova, they obtained a constraint of $L \leqslant 70$ MeV[52] shown by a solid line with an arrow indicating the direction of the bound in Fig. 5, labeled "NS grav. binding energy (Newton & Li, 2009)").

Steiner and Watts[53] have shown that the fundamental seismic shear mode, observed as a quasiperiodic oscillation in giant flares emitted by highly magnetized neutron stars, is particularly sensitive to the nuclear physics of the crust. Since the properties of neutron star crust are sensitive to the density dependence of the symmetry energy (See, e.g., Ref. [54]), the crust oscillations of neutron stars provide a unique probe of the symmetry energy[55]. Indeed, Sotani et al.[56] have general-relativistically calculated the frequency of fundamental torsional oscillations of neutron star crusts, and found that the calculated frequency is sensitive to the density depen-

dence of the symmetry energy, but almost independent of the incompressibility of symmetric nuclear matter. By identifying the lowest-frequency quasi-periodic oscillation in giant flares observed from soft gamma-ray repeaters as the fundamental torsional mode and allowing for the dependence of the calculated frequency on stellar models, they obtained a constraint of $L \geqslant 50$ MeV[56] shown by a dashed line with an arrow indicating the direction of the bound in Fig. 5, labeled "NS crust osc. (Sotani *et al.*, 2012)". In a sequent work, Sotani *et al.*[57] considered the effects of superfluidity of dripped neutrons in the crust of a neutron star on the frequencies of the crust's fundamental torsional oscillations, and they obtained a new constraint $L = 100 \sim 130$ MeV[57] shown by a band with slanted line in Fig. 5, labeled "NS crust osc. (a) (Sotani *et al.*, 2013)". A similar constraint $L = 101.1 \sim 131.0$ MeV (not shown in Fig. 5) has been obtained more recently by Sotani *et al.*[58] from a systematic study on the fundamental frequencies of shear torsional oscillations in neutron star crusts. Alternatively, if only the second lowest frequency observed in SGR 1 806.20 has a different origin, they obtained another constraint $L = 58.1 \sim 85.3$ MeV[58] shown by the gray band in Fig. 5, labeled "NS crust osc. (b) (Sotani *et al.*, 2013)".
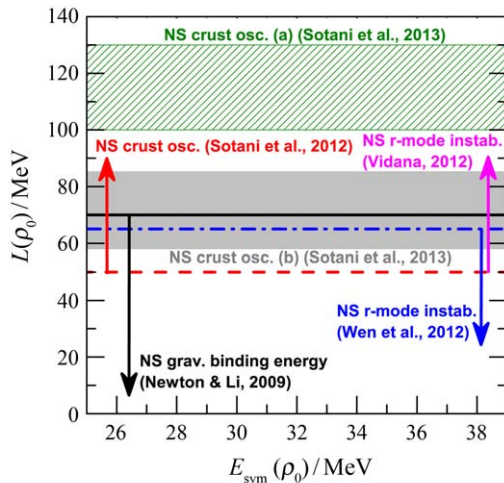

Fig. 5 (color online) Constraints on $E_{\mathrm{sym}}(\rho_0)$ and L from the gravitational binding energy, crust oscillations and r-mode instability of neutron stars. The arrows indicate the direction of the bound. See text for details.

The r-mode instability provides a possible mech-

anism to limit neutron star spin-up and thus explains why the observed maximum rotation frequency of known pulsar is only 716 Hz, significantly less than the Kepler frequency (beyond which material will be ejected from the equator of the star) of about 2 000 Hz or above predicted by conventional neutron star models. The onset of the r-mode instability is essentially determined by the competition between the core viscosity which damps the mode, and the driving force caused by the gravitational radiation. Usually the r-mode amplitude is largest at the crust-core boundary which is essentially controlled by the symmetry energy (*i.e.*, the L parameter). Therefore, the r-mode instability window is sensitive to the symmetry energy. Indeed, using a consistent description of the crust-core transition density and the core EOS, Wen *et al.*[59] have explored the L parameter dependence of the r-mode instability window, and they obtained a constraint $L \leqslant 65$ MeV to be consistent with the observed pulsars in low-mass X-ray binaries (LMXBs), shown by a dash-dotted line with an arrow indicating the direction of the bound in Fig. 5, labeled "NS r-mode instab. (Wen *et al.*, 2012)". On the other hand, using a similar analysis, Vidana [60] also obtained a constraint of $L \geqslant 50$ MeV, shown by a dashed line with an arrow indicating the direction of the bound in Fig. 5, labeled "NS r-mode instab. (Vidana, 2012)". As pointed out by Newton *et al.*[51], the difference between these two constraints could be due to the fact that the latter takes into account viscous dissipation throughout the whole core while the former takes only at the crust-core boundary layer. Moreover, the latter does not consistently calculate the neutron star core and crust together, and the radius is varied independently of both, even though the radius strongly correlated with crust thickness and core composition.

3.4 Discussions

In Figs. $1 \sim 5$, we have included totally 30 constraints on L and $E_{\mathrm{sym}}(\rho_0)$, in particular, 5 from heavy ion collisions, 2 from optical model potential, 6 from nuclear mass, 1 from isobaric analog state energies, 2 from nuclear neutron skin thickness, 2 from nuclear pygmy dipole resonance, 6 from mass and

radius of neutron stars, 1 from gravitational binding energy of neutron stars, 3 from crust oscillations of neutron stars, and 2 from the r-mode instability of neutron stars. Obviously, it cannot be that all the constraints are equivalently reliable since some constraints do not have any overlap.

It should be emphasized that the symmetry energy cannot be directly measured experimentally and each constraint shown in Figs. 1 ∼ 5 have been obtained within a certain theoretical model with some approximations or special assumptions, and thus the model dependence of the constraints is unavoidable. To better understand the model dependence of the constraints and reduce the uncertainties is thus of critical importance.
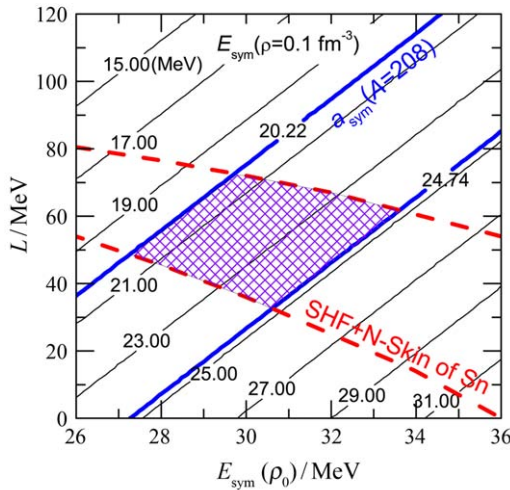

Fig. 6　(color online) Contour curves in the $E_{sym}(\rho_0)$ -L plane for $E_{sym}(\rho = 0.1 \text{ fm}^{-3})$ from SHF calculations.

　　The region between the two thick solid lines represents the constraint obtained with 20.22 MeV ⩽ $E_{sym}(\rho_A = 0.10 \text{ fm}^{-3})$ ⩽ 24.74 MeV while the region between the two thick dashed lines is the constraint from the SHF analysis of neutron skin data of Sn isotopes within a 2σ uncertainty [43]. The shaded region represents the overlap of the two constraints. Taken from Ref. [34].

We would like to highlight two constraints described above, i.e., "$E_{sym}(\rho_A = 0.1 \text{ fm}^{-3})(2011)$" in Fig. 2 and "SHF+N-Skin (2010)" in Fig. 3 since both constraints have been obtained within the same theoretical framework of SHF with 95% confidence. The two constraints are re-plotted in Fig. 6. It is very interesting to see that while the constraint

"$E_{sym}(\rho_A = 0.1 \text{ fm}^{-3})(2011)$" indicates a linear positive correlation between L and $E_{sym}(\rho_0)$, the constraint "SHF+N-Skin (2010)" displays a negative correlation. Actually, only the constraint "SHF+N-Skin (2010)" among the 30 constraints described above displays such negative correlation. This interesting feature makes the constraint "SHF+N-Skin (2010)" particularly important as combing it with other constraints will significantly improve the constraint on L and $E_{sym}(\rho_0)$ simultaneously. It is interesting to see that the overlap of "SHF+N-Skin (2010)" and "$E_{sym}(\rho_A = 0.1 \text{ fm}^{-3})(2011)$" is consistent with all the other constraints described above except "IAS+LDM (2009)". The latter neglected the higher-order density curvature contribution of the symmetry energy and its inclusion may reduce the L value[36] (See also Ref. [34]).

The positive correlation between L and $E_{sym}(\rho_0)$ from "$E_{sym}(\rho_A = 0.1 \text{ fm}^{-3})(2011)$" has been clearly demonstrated in Ref. [34] where it has been shown that a fixed value for the magnitude of the symmetry energy at a subsaturation density will lead to a positive correlation between L and $E_{sym}(\rho_0)$. This feature implies that nuclear mass fitting should lead to positive correlation between L and $E_{sym}(\rho_0)$ since $E_{sym}(\rho_A = 0.1 \text{ fm}^{-3})$ essentially reflects the symmetry energy part of medium and heavy nuclei, which is further demonstrated by the nice agreement between the constraints "$E_{sym}(\rho_A = 0.1 \text{ fm}^{-3})(2011)$" and "Nucl. Mass(2012)" as shown in Fig. 2.

The negative correlation between L and $E_{sym}(\rho_0)$ from "SHF+N-Skin (2010)" can be understood from the fact that the neutron skin thickness is physically related to the neutron and proton pressure difference at sub-saturation density corresponding to the characteristic (average) density of finite nuclei, which is essentially controlled by the density slope of symmetry energy at sub-saturation density (rather than L at saturation density). Indeed, Zhang and Chen[61] recently demonstrated that the neutron skin thickness of heavy nuclei is uniquely fixed by the symmetry energy density slope $L(\rho)$ at a sub-saturation cross density $\rho_c \approx 0.11 \text{ fm}^{-3}$ rather than at saturation density. Furthermore, they found that

a fixed value of $L(\rho_c)$ leads to a negative $E_{sym}(\rho_0)$-$L(\rho_0)$ correlation[61], providing an explanation why the data of neutron skin thickness alone leads to negative correlation between L and $E_{sym}(\rho_0)$.

From Figs. 1 ∼ 5, one can see that while $E_{sym}(\rho_0)$ and L can vary largely depending on the data or methods, all the constraints are consistent with $E_{sym}(\rho_0) = (32.5 \pm 2.5)$ MeV and $L = (55 \pm 25)$ MeV. At this point, it should be mentioned that $E_{sym}(\rho_0)$ and L have also been extracted from the EOS of pure neutron matter obtained from chiral effective field theory calculations[62−63] and quantum Monte Carlo techniques[64−65] with realistic two- and three-nucleon interactions. The advantage of such microscopic calculations for the EOS of pure neutron matter is that the uncertainties can be estimated and controlled. It is interesting to note that the extracted $E_{sym}(\rho_0)$ and L from chiral effective field theory calculations[62−63] and quantum Monte Carlo techniques[64] are nicely in agreement with the center values of $E_{sym}(\rho_0) = (32.5 \pm 2.5)$ MeV and $L = (55 \pm 25)$ MeV.

It should be also mentioned that the center values of $E_{sym}(\rho_0) = (32.5 \pm 2.5)$ MeV and $L = (55 \pm 25)$ MeV, are further in agreement with the most recent analysis of the existing data on neutron skin thickness of Sn isotopes and the binding energy difference for a number of heavy isotope pairs within the SHF approach[61], the analysis of the isospin diffusion, n/p ratio and double n/p ratio in hevay ion collisions with a new version of ImQMD based on a full Skyrme energy density functional[66], and the isobaric analog state energies together with the measurement of neutron skin thickness of ^{48}Ca and ^{207,208}Pb[67−68].

4   The symmetry energy at supra-saturation densities

While significant progress has been made on constraining the symmetry energy around the saturation density, the high density behavior of the symmetry energy remains elusive and largely controversial. FOPI data on the π^-/π^+ ratio in central heavy-ion collisions at SIS/GSI energies favor a quite soft symmetry energy at $\rho \geqslant 2\rho_0$ from the isospin and momentum dependent IBUU04 model analysis[12] while an opposite conclusion has been obtained from the improved isospin dependent quantum molecular dynamics (ImIQMD) model analysis[13]. A more recent analysis of FOPI data on the π^-/π^+ ratio based on the isospin dependent Boltzmann‐Langevin approach [69] indicated a quite soft symmetry energy at $\rho \geqslant 2\rho_0$, consistent with the IBUU04 model analysis. It should be mentioned that the ImIQMD model analysis did not consider the energy dependent symmetry potential and it cannot explain qualitatively the isospin fractionation phenomenon observed in heavy ion collisions[70−71]. A further careful check is definitely necessary to understand the model dependence. Recently, Xu et al.[72] studied the pion in-medium effect on the charged-pion ratio in heavy-ion collisions at various energies within the framework of a thermal model with its parameters fitted to the results from an isospin-dependent BUU transport model, and they found that the pion in-medium effects reduce the π^-/π^+ ratio in high-energy heavy-ion collisions compared to that using free pions, especially at lower incident energies. Therefore, to understand quantitatively the symmetry energy effect on pion production in heavy-ion collisions, it is important to include the isospin-dependent pion in-medium effects, although this is highly nontrivial in the transport model.

By analyzing the elliptic-flow ratio of neutrons with respect to protons or light complex particles from the existing FOPI/LAND data for ^{197}Au + ^{197}Au collisions at 400 MeV/u within the UrQMD model, Russotto et al.[14] obtained a moderately soft symmetry energy with a density dependence of the potential term proportional to $(\rho/\rho_0)^\gamma$ with $\gamma = 0.9 \pm 0.4$. In a more recent work, Cozma et al.[73] analyzed the experimental FOPI/LAND data of neutron-proton elliptic flow difference and ratio for ^{197}Au + ^{197}Au collisions at 400 MeV/u within the Tubingen QMD model by using a parametrization of the symmetry energy derived from the momentum dependent Gogny force, they extracted a moderately stiff symmetry energy.

Besides using heavy ion collisions to constrain the supra-saturation density behavior of the symme-

try energy, it has been also proposed recently[74] that the three bulk characteristic parameters $E_{\text{sym}}(\rho_0)$, L and K_{sym} essentially determine the symmetry energy with the density up to about $2\rho_0$. This opens a new window to constrain the supra-saturation density behavior of the symmetry energy from its precise knowledge around saturation density.

5　Summary

Significant progress has been made both experimentally and theoretically on constraining the density dependence of the symmetry energy after more than one decade of studies in the community. We have summarized the existing constraints on the density dependence of the symmetry energy, especially its magnitude $E_{\text{sym}}(\rho_0)$ and its density slope L at saturation density. Although the values of $E_{\text{sym}}(\rho_0)$ and L can vary largely depending on the data or models, all the constraints obtained so far from nuclear reactions, nuclear structures, and the properties of neutron stars are consistent with $E_{\text{sym}}(\rho_0) = (32.5 \pm 2.5)$ MeV and $L = (55 \pm 25)$ MeV. More high quality data and more accurate theoretical methods are needed to further reduce the theoretical and experimental uncertainties of the constraints on $E_{\text{sym}}(\rho)$ around the saturation density. In contrast, the determination of the supra-saturation density behavior of the symmetry energy is still largely controversial and remains a big challenge in the community.

References:

[1]　LATTIMER J M, PRAKASH M. Science, 2004, **304**: 536; LATTIMER J M, PRAKASH M. Phys Rep, 2007, **442**: 109.

[2]　STEINER A W, PRAKASH M, LATTIMER J M, *et al.* Phys Rep, 2005, **411**: 325.

[3]　BARAN V, COLONNA M, GRECO V, *et al.* Phys Rep, 2005, **410**: 335.

[4]　CHEN L W, KO C M, LI B A, *et al.* Front Phys China, 2007, **2**: 327. [arXiv:0704.2340].

[5]　LI B A, CHEN L W, KO C M. Phys Rep, 2008, **464**: 113.

[6]　TSANG B M, STONE J R, CAMERA F, *et al.* Phys Rev C, 2012, **86**: 015803.

[7]　LATTIMER J M. Ann Rev Nucl Part Sci, 2012, **62**: 485.

[8]　LI B A, CHEN L W, FATTOYEV F J, *et al.* J Phys: Conf Series, 2013, **413**: 012021. [arXiv:1212.1178].

[9]　HOROWITZ C J, POLLOCK S J, SOUDER P A, *et al.* Phys Rev C, 2001, **63**: 025501.

[10]　SIL T, CENTELLES M, VIÑAS, *et al.* Phys Rev C, 2005, **71**: 045502.

[11]　WEN D H, LI B A, CHEN L W. Phys Rev Lett, 2009, **103**: 211102.

[12]　XIAO Z G, LI B A, CHEN L W, *et al.* Phys Rev Lett, 2009, **102**: 062502.

[13]　FENG Z Q, JIN G M. Phys Lett B, 2010, **683**: 140.

[14]　RUSSOTTO P, WU P Z, ZORIC M, *et al.* Phys Lett B, 2011, **697**: 471.

[15]　XU C, LI B A. Phys Rev C, 2010, **81**: 064612.

[16]　CHEN L W. Proceedings of the 14th National Conference on Nuclear Structure in China (NSC2012)[C]//MENG J, SHEN C W, ZHAO E G, ZHOU S G (Editors). Singapore: World Scientific, 2012: 43–54 [arXiv:1212.0284].

[17]　CAI B J, CHEN L W. Phys Rev C, 2012, **85**: 024302.

[18]　CHEN L W, KO C M, LI B A. Phys Rev Lett, 2005, **94**: 032701; LI B A, CHEN L W. Phys Rev C 2005, **72**: 064611.

[19]　TSANG M B, LIU T X, SHI L J, *et al.* Phys Rev Lett, 2004, **92**: 062701.

[20]　CHEN L W, KO C M, LI B A. Phys Rev C, 2005, **72**: 064309.

[21]　TSANG M B, FRIEDMAN W A, GELBKEL C K, *et al.* Phys Rev Lett, 2001, **86**: 5023.

[22]　SHETTY D, YENNELLO, S J, SOULIOTIS G A. Phys Rev C, 2007, **75**: 034602.

[23]　TSANG M B, ZHANG Y X, DANIELEWICZ, *et al.* Phys Rev Lett, 2009, **102**: 122701.

[24]　SUN Z Y, TSANG M B, LYNCH W G, *et al.* Phys Rev C, 2010, **82**: 051603(R).

[25]　KOHLEY Z, MAY L W, WUENSCHEL S, *et al.* Phys Rev C, 2010, **82**: 064601.

[26]　XU C, LI B A, CHEN L W. Phys Rev C, 2010, **82**: 054607.

[27]　XU C, LI B A, CHEN L W, KO C M. Nucl Phys A, 2011, **865**: 1.

[28]　CHEN R, CAI B J, CHEN L W, *et al.* Phys Rev C, 2012, **85**: 024305.

[29]　CAI B J, CHEN LW. Phys Lett B, 2012, **711**: 104.

[30] LI X H, CHEN L W. Nucl Phys A, 2012, **874**: 62.

[31] LI X H, CAI B J, CHEN L W, et al. Phys Lett B, 2013, **721**: 101.

[32] MYERS W D, SWIATECKI W J. Nucl Phys A, 1996, **601**: 141.

[33] LIU M, WANG N, LI Z X, et al. Phys Rev C, 2010, **82**: 064306.

[34] CHEN L W. Phys Rev C, 2011, **83**: 044308.

[35] MOLLER P, MYYERS W D, SAGAWA H, et al. Phys Rev Lett, 2012, **108**: 052501.

[36] LATTIMER J M, LIM Y. ApJ, 2013, **771**: 51.

[37] JIANG H, FU G J, ZHAO Y M, et al. Phys Rev C, 2012, **85**: 024301.

[38] AGRAWAL B K, DE J N, SAMADDAR S K, et al. Phys Rev C, 2013, **87**: 051306(R); AGRAWAL B K, DE J N, SAMADDAR S K. Phys Rev Lett, 2012, **109**: 262501.

[39] DANIELEWICZ P. Nucl Phys A, 2003, **727**: 233.

[40] DANIELEWICZ P, LEE J. Nucl Phys A, 2009, **818**: 36.

[41] BROWN B A. Phys Rev Lett, 2000, **85**: 5296; TYPEL S, BROWN B A. Phys Rev C, 2001, **64**: 027302.

[42] CENTELLES M, ROCA-MAZA X, VINAS X, et al. Phys Rev Lett, 2009, **102**: 122502; WARDA M, VINAS X, ROCA-MAZA X, et al. Phys Rev C, 2009, **80**: 024316.

[43] CHEN L W, KO C M, LI B A, et al. Phys Rev C, 2010, **82**: 024321.

[44] PIEKAREWICZ J. Phys. Rev. C, 2006, **73**: 044325.

[45] KLIMKIEWICZ, A, PAAR N, ADRICH P, et al. Phys Rev C, 2007, **76**: 051603(R).

[46] CARBONE A, COLÒ G, BRACCO A, et al. Phys Rev C, 2010, **81**: 041301(R).

[47] LATTIMER J M, PRAKASH M. ApJ, 2001, **550**: 426.

[48] STEINER A W, LATTIMER J M, BROWN E F. ApJ, 2010, **722**: 33.

[49] STEINER A W, GANDOLFI S. Phys Rev Lett, 2012, **108**: 081102.

[50] STEINER A W, LATTIMER J M, BROWN E F. ApJ, 2013, **765**: L5.

[51] NEWTON W G, GEARHEART M, WEN D H, et al. J Phys: Conf. Series, 2013, **420**: 012145.

[52] NEWTON W G, LI B A. Phys Rev C, 2009, **80**: 065809.

[53] STEINER A W, WATTS A L. Phys Rev Lett, 2009, **103**: 181101.

[54] XU J, CHEN L W, LI B A, et al. Phys Rev C, 2009, **79**: 035802; XU J, CHEN L W, LI B A, et al. ApJ, 2009, **697**: 1549.

[55] GEARHEART M, NEWTON W G, HOOKER J, et al. MNRAS, 2011, **418**: 2343.

[56] SOTANI H, NAKAZATO K, IIDA K, et al. Phys Rev Lett, 2012, **108**: 201101

[57] SOTANI H, NAKAZATO K, IIDA K, et al. MNRASL, 2013, **428**: L21.

[58] SOTANI H, NAKAZATO K, IIDA K, et al. MNRAS, 2013 [arXiv:1303.4500v2].

[59] WEN D H, NEWTON W G, LI B A. Phys Rev C, 2012, **85**: 025801.

[60] VIDANA I, Phys. Rev. C, 2012, **85**: 045808.

[61] ZHANG Z, CHEN L W. Phys Lett B, 2013, **726**: 234.

[62] HEBELER K, LATTIMER J, PETHICK C, et al. Phys Rev Lett, 2010, **105**: 161102.

[63] TEWS I, KRUGER T, HEBELER K, et al. Phys Rev Lett, 2013, **110**: 032504.

[64] GANDOLFI S, CARLSON J, REDDY S. Phys Rev C, 2012, **85**: 032801(R).

[65] GEZERLIS A, TEWS I, EPELBAUM E, et al. Phys Rev Lett, 2013, **111**: 032501.

[66] ZHANG Y X, LI Z X. private communications, 2013.

[67] DANIELEWICZ P. private communications, 2013.

[68] DANIELEWICZ P, LEE J. Nucl Phys A, 2014, **922**: 1.

[69] XIE W J, SU J, ZHU L, et al. Phys Lett B, 2013, **718**: 1510.

[70] XU H S, TSANG M B, LIU T X, et al. Phys Rev Lett, 2000, **85**: 716.

[71] LI B A. Phys Rev Lett, 2002, **88**: 192701.

[72] XU J, CHEN L W, KO C M, et al. Phys Rev C, 2013, **87**: 067601.

[73] COZMA M D, LEIFELS Y, TRAUTMANN W, et al. arXiv:1305.5417v1, 2013.

[74] CHEN L W. Science China: Physics, Mechanics and Astronomy, 2011, **54**: s124. [arXiv:1101.2384].

对称能研究进展

陈列文[1, 2, 1)]

（ 1. 上海交通大学物理与天文系，上海 200240；
2. 兰州重离子加速器国家实验室原子核理论中心，兰州 730000 ）

摘要：   总结了目前基于分析地面实验室以及天文观测数据所得到的关于核物质对称能密度相关性的约束。结果表明，在核物质饱和密度 ρ_0 处，关于对称能的大小 $E_{\mathrm{sym}}(\rho_0)$ 及其密度梯度参数 L 的不同具体约束强烈地依赖于不同的实验数据或理论方法。另一方面，所有存在的约束都和 $E_{\mathrm{sym}}(\rho_0) = (32.5 \pm 2.5)$ MeV 以及 $L = (55 \pm 25)$ MeV 一致。如何确定核物质对称能的高密行为仍然是一个挑战。

关键词：   对称能；非对称核物质状态方程；核反应；核结构；中子星